UNIVERSITÀ POLITECNICA DELLE MARCHE

FACOLTÀ DI INGEGNERIA

Dipartimento di Ingegneria dell'Informazione

Master's degree in BIOMEDICAL ENGINEERING

EMG-data Driven Model for Wrist Joint Motion Estimation

Supervisor:

Prof. Sandro Fioretti

Author:

Giacomo Verde

Co-supervisor:

Ing. Alessandro Mengarelli

Ing. Andrea Tigrini

Academic year: 2020-2021

INDEX

Acknowledgements

For the development of this thesis, I would like to thank my Supervisor Sandro Fioretti, co-Supervisors Alessandro Mengarelli and Andrea Tigrini, and Professor Federica Verdini for helping me constantly and efficiently during my research internship and for reviewing the present manuscript. Moreover, I would like to strongly thank my fellow students Alessio Di Lello, Federico Barbarossa and Giacomo Covella. Special thanks to my family and my friends for supporting me over these years.

Abstract

Introduction. This thesis aims to investigate the performance of free-model techniques in continuous wrist motion estimation, using forearm muscle EMG signals. More in details, we compare the performance of feature-based models and signal-driven models in predicting two different types of motion: wrist flexion/extension and wrist adduction/abduction. Differently from the common literature set-up, in which single-unite surface electrodes are used, we acquire forearm EMG signal using a wearable device. Comparison between our results and similar literature study results is successively done to assess the validity of this set-up in wrist angle estimation experiment.

Material and Methods. 6 healthy subjects are asked to complete two different wrist motion tasks: firstly, a flexion/extension task and in a second time an adduction/abduction task. Forearm muscles EMGs are acquired using OYMotion GForcePro+, while wrist cinematic ones, used as regression targets, are acquired using a next generation inertial measurement unit (NGIMU). Once the EMG signals are processed and segmented, 4 time-domain features (Hudgins' set) and one frequency-domain features are extracted. These latter are used to train and validate the model outcoming from Random Forest (RF) algorithm, while a Convolutional Neural Network (CNN) is trained and validate using the processed EMG signals. Performance metrics are calculated to evaluate the estimation performances both in training and testing phase.

Results and Discussion. The outcomes of this study show the CNN has better performances with respect to the RF algorithm, both in training and testing phase and in prediction of both wrist motion tasks. The lower performance in feature-based model (RF) can be attributed to the extraction of low discriminative features, despite Hudgins' set is considered a gold standard approach in this type of studies. Moreover, comparing the obtained performance metrics with those found in similar literature studies, the implementation of wearable device is demonstrated to be a valid option to surface electrodes in wrist motion estimation experiment.

1 Introduction

The human hand is a powerful tool for sensing and operating in the environment, as well as a very sophisticated means for physical and social interaction. It allows the human beings to accomplish sophisticated movements, from power to precision tasks, thanks to the large number of Degrees of Freedom (DoF) (21 DoF for the hand and 6 for the wrist) and the paramount role played by thumb opposition. Hand loss can be perceived as a devastating damage since it affects the level of autonomy, limiting the capability of performing working, social, and daily living activities (ADLs). Approximately 3500 and 5200 upper limb amputations are reported each year in Italy and in UK, respectively, with forearm amputation being one of the most occurring [1].

In this latter case, a trans-radial approach is generally followed, and it consists in an amputation that can occur at different levels from elbow to wrist. The goal of trans-radial amputation is to preserve as much length as possible, as this directly correlates with the amount of pronation-supination that can occur [2]. This is a crucial feature in maintaining the functional ability of the limbs and consequently of the prostheses. It can range from 120 degree for wrist disarticulations, down to 0 for very short stump lengths. The second aim of trans-radial amputation is preservation of the ulna to a minimum of 5 cm for the fitting of prosthesis [2]. Indeed, the amputation procedure is followed by period of rehabilitation, during which the amputees are helped to reconstruct lost functions of hands, thanks to the application of prostheses. These can be classified into two main groups: cosmetic prostheses and functional prostheses. The first one won't provide any function to the patient, but it will take the place of the missing limb giving the appearance of a normal arm both to the sight and touch. For what concern the functional prostheses they can be divided in body-powered and bioelectric. Body-powered prostheses system are mechanical device, designed to work without any electronics and to allow the user to operate the terminal device by flexing a muscle near the stump of the amputated limb. The energy from this movement is then transferred to the prosthesis by means of a stainless-steel cable. The strong point of such a mechanism is the possibility of controlling the effort. When grasping, the user themself determines the compression strength, its speed and can sense resistance, when the wrist rests on the object. Alternatively, there are the bioelectric prostheses, also called myoelectric, which are the state-of-the-art for hand prostheses. The stump-receiving socket has built-in myo-sensors that read the EMGs coming from the residual muscle of the forearm. Then, this information is transmitted to the wrist microprocessor of the prostheses, and as a result, it's possible to move the fingers of the prosthetic hand, performing a certain gesture or even grasping objects. Hence, the myo-electric prostheses are controlled by signals emerging when the muscles contract.

Indeed, Electromyography (EMG) signals provides information related to the muscles' activities and can be used to exploited for the user's motion intention estimation.

Several EMG based systems were proposed for estimating the hand and wrist motions and were used consequently as an interface, not only for prosthetic device, but also for controlling wrist exoskeletons [3][4], for teleoperating robotic arms [5][6] or in a virtual environment to control computer-animated hands [7].

In order to estimate and control the wrist motion, researchers have primarily focused on classification-based methods. All these approaches investigate a discrete classification of the wrist or hand/fingers opening and closing. For instance, in [7] [8] [9], the authors propose methods for classifying different types of movements including flexion/extension of the wrist as well as flexion/extension of a different combination of fingers.

In Murray C. book [10], the author addresses the question of prosthesis design and acceptance from the consumers' perspective and points out their need to control the wrist. Once the grasp is performed, and in order to manipulate the corresponding object without having to move the whole arm, one needs to be able to control the wrist joint angles smoothly and continuously which could not be ensured through classification techniques. With this purpose, in the past two decades, researchers investigated many different techniques of regression, which have the potential, using the information carried out by the EMG signals, to estimate in a continuous way, one DoF wrist motion, two DoF wrist motion and three DoF wrist motion [11]. In the following paragraphs, it will be given a general explanation of the different regression techniques and an overview of the state of the art in wrist angle estimation.

1.1 Wrist angle continuous estimation techniques

Functional hand prostheses have traditionally been limited to single-degree-of-freedom devices. In contrast, the human hand is extensively articulated, possessing approximately twenty major degrees of freedom which allow it to execute a wide variety of grasps and postures. The associated disparity in performance and appearance between the human hand and these traditional replacements is guiding latest studies to create more complex devices capable of guarantee greater functionality and mobility. In the past decade, many studies are brought on with the purpose on increasing the degree of freedom for wrist motion which was barely taken in consideration before. The final purpose is to create devices capable of replicating the mobility of the wrist, guarantying the user to execute flexion extension and add-abduction movement in a continuous pattern. In literature there are much researches centered on the estimation of the wrist angle of motion starting from the acquisition of EMG signals of the forearm muscles.

EMG based continuous limb motion estimation approaches can be categorized into two subsets, model-free and model based.

- Model-based approaches have been widely applied trying to provide an explicit representation between the EMG signal and muscle forces, joint moments, and/or joint kinematics from EMG signals. This technique generally consists of a four-step process. In the first step, muscle activation dynamics govern the transformation from the EMG signal to a measure of muscle activation. In the second step, muscle contraction dynamics characterize how muscle activations are transformed into muscle forces. The third step requires a model of the musculoskeletal geometry to transform muscle forces to joint moments. Finally, the equations of motion allow joint moments to be transformed into joint movements [12] .

  In these types of approach there are mainly two focal points. The first one is the correct definition of a musculoskeletal model, in which the structure and function of the muscle are modeled using analogues electrical and mechanical components, in order to guarantee an optimal simulation of the general muscle activation. The second one is the estimation of the intrinsic physiological parameter of the muscle, required by the model. This is a crucial point because this step is responsible for the calibration and differentiation of the model depending on the subject from which we are acquiring EMG signal. If on one side, this type of approach reduces the acquirement of training data to a small amount in order to calibrate the model, on the other hand the many unknown physiological parameters for each muscle increase greatly the complexity of the model [13]. Moreover, using few muscles to establish the musculoskeletal model may overestimate the physiological parameters, for example, the parameters may exceed the physiological range when these muscles are assumed to be the only muscle groups contributing to the joint motion [14]. For this reason, another crucial point is the choice of how many muscles are needed to be model for a correct representation of the motion task.

- Model-free approaches involve techniques consisting of mapping the relationship between EMG signals and the desired motion by the numerical functions. Thanks to this approach we are able to overcome the difficulties encountered in the model-based approach regarding the definition of the physiological parameters. However, there are still some limitations. It is a 'black box' method, employing a general map function rather than explicitly revealing the functional relationships between neuro-commands and the corresponding motion [15] Secondly, a large amount of data, as well as the related motions, is required to train the model to interpret the prediction with given EMG signals and in order to predict a certain motion,

we need to train the model with set of data related to the same motion [16]. There are two different types of approaches: Feature-driven and signal-driven regression. In the first case regression models are trained only using selected features, which are computed from the acquired EMG signal, following precise rules of feature extraction [17], [18]. Instead, signal-driven models are trained using the totality of raw data of EMG acquisition, from which the regressors are able to find signal patterns and characteristics that allows to predict the desired motion. In this case, the time-consuming procedure of feature extraction and selection will be avoided.

1.2 State of the art in wrist angle estimation using regression algorithms

In this study, the focus was pointed on the model-free approach, since it appears to be a more intuitive technique with respect the model-based ones, even though a large amount of data is required for an optimal training phase. Regression technique can be categorized into two main groups feature-based model and signal-driven model. A quick explanation of the approach used in these methods and the related studies found in literature are reported below.

- For what concern feature-driven model, the usual procedure, after the preprocessing of EMG signals, consist of two steps: feature extraction and regression.

  After the data recording, the acquired samples are converted into features which are used for regression. There are many feature extraction methods which are applied on raw EMG, to carry out actual EMG signal, such as time series analysis, Wavelet Transform, Discrete Wavelet Transform, Wavelet Packet Transform, Fast Fourier Transform, Discrete Fourier Transform [19]. Then, on the transformed signal it's possible to compute the desired features, depending on the own necessities, choosing between time domain feature, frequency domain feature and time frequency domain feature. Among all, features in time domain are the most used since are the most quick and easy to implement. Indeed, these features do not need any transformation, since they are computed on the raw EMG time series. [18]. However, feature extraction is relevant because it determines the ceiling of the recognition performance, which aims to provide a feature set that is optimal for representing the information from EMG.

  In this type of approach, one of the most common regressor is the support vector machine model (SVM), due to its good performance in non-linear estimation and fast convexity for real time implementation [20].

  Although there are still few studies about it, general outcomes are of good auspice. Hong-Bo Xie et al. compared the performance of SVM and Artificial Neural Network (ANN) models in

task of wrist extension. It was demonstrated that the wrist angles measured and predicted by SVM could hardly be distinguished, and the experimental results indicated that the SVM model performed better in comparison with the ANN models [21]. Jun Shi et al. compared the performance of one and two element linear regression and SVM model used in prediction of wrist flexion task and wrist extension task. Also, in this case SVM model had better results, that could be increased with the usage a larger training data set, and for this reason it was demonstrated that it was more adaptive than the multi-element linear regression, thanks to better performance [22]. S. El-Khoury et al instead used SVM models trying to predict wrist circular trajectories. These circular motions were chosen in order to make sure that the subjects were exploring the whole reachable space of their wrist. Consequently, two angles were predicted by the regression model, the abduction/adduction and flexion/extension angles. Despite the high complexity task, the SVM shown acceptable results and a good generalization across several days while performing the experiment on the same subject [20].

- Signal-driven models are mainly Deep learning (DL) models. Unlike feature-based algorithms, which need to extract features from input data for classification or regression tasks, DL methods can extract high-level features automatically from raw input data while using multiple hidden layers. In recent years, the DL-based scheme has been widely used in EMG recognition. Many pieces of research have applied deep neural networks for EMG processing. Despite the few studies in literature, the model that allowed to obtain the best results in term of wrist motion prediction is convolutional neural network (CNN) [23]. Indeed, in the recent years, two important studies demonstrate the strength of CNN with respect classic machine learning technique. Ameri et al. decode 2 DOF wrist movements (flexion, extension, pronation, supination and combination of them) using the Fitts' law test, for online application, with a regression CNN. This outperforms the support vector regression (SVR) based method with five EMG features as input [24]. Bao et al. estimated 3-DOF movement of the wrist (flexion, extension, adduction, abduction, pronation, supination and combination of them) using a spectrum image of the EMG. Several feature-based methods are compared with the proposed CNN, and the performance demonstrates the superiority of the CNN-based method [11].

1.3 EMG acquisition devices

As said previously, model free approaches require large amount of data to be given in input to the models as training data. For this reason, the phase of acquisition is extremely important, and the choice of the EMG recording devices will influence the quality acquired signals.

The most used are the surface electrodes These electrodes are designed to measure potentials from the surface of the skin being the less invasive for the patient. They are available in many forms and sizes. Using surface electrodes, EMG is recorded from discrete sites on a muscle and thus provides only a limited picture of the actual muscular electrical activity on which the electrode is placed. Moreover, to reach higher density EMG signal recordings it's possible to use multi-channel grid electrode, matrix of electrodes of 1mm diameter, placed apart, arranged in adjacent arrays. For example, J. M. Hahne et al. for the acquisition of EMG signals during task of wrist flexion extension, used a 192-channel electrode grid (ELSCH064NM 3–3, OT Bioelectronic, 8 24 channels, 10 mm inter-electrode-distance). The electrode array was placed on the proximal portion of the left forearm, covering a range of 8 cm [25].

However, the high cost of production doesn't make multi-channel grid electrodes accessible to everyone. Moreover, when using surface electrodes, placement is a crucial point, since in case of wrong positioning, there could be redundant acquisitions or more easily they could slip causing incorrect measurements due to shifting. Another disadvantage, from a structural point of view, is that the traditional EMG electrodes are connected to the recording system with various channel wires, which could limit user activity boundary and/or hinder the user's movement

To overcome these negative aspects, a good solution, which is a compromise in terms of cost and spatial resolution and don't require any careful application, is represented by wearable devices. Many industries started to commercialize these types of devices. One of the greatest advantages is, beyond the before mentioned ones, the intuitive approach for the usage due to its wearability. Indeed, these devices make the acquisition of the signals more easy and faster, reducing the time, usually required for preparing the patient and applying the electrodes. For what concern the acquisition of EMG signals from the upper limb, one of the most diffused and comfortable solution is a wearable device built to be wore as an armband, where an array of electrodes is arranged along the internal surface to be in contact with skin once wore by the user.

1.4 Aim of the study

The main goal of this research is the performance comparison in wrist motion estimation using feature-driven technique and signal-driven technique, starting from the surface EMG signals acquisition of the forearm muscles. The evaluation will be done on prediction of flexion extension and adduction abduction tasks, executed in a cyclic manner and with variable range. Differently from what is found in literature, we introduced the usage, for the first time, of a wearable device, in this case the OYMotion GForcePro+, to acquire the EMG signals of the forearm muscles. The evaluation of the results obtained in testing phase, compared with those found in similar literature study, will assess also if wearable devices, instead of normal surface electrodes, can provide enough good quality EMG data for a consistent training of the features-driven model and signal-driven model. The following 4 macro-sections of this thesis are Materials and methods (chapter 2) that describes in detail the setup and hardware used, the wrist motion task, the signal processing phase, the extraction of features and the regressors used. Results (chapter 3) is the section dedicated to all the results that we have carried out from experiments while in Discussion and Conclusion (chapter 4), the results are thoroughly explained and discussed.

2 Material and methods

2.1 Forearm muscles

The activation of forearm muscles allows to execute precise movement of the hand, within a variable range, at the level of the wrist joint. This is possible because the forearm is a high muscular density compartment. Indeed, there are twenty different muscles of the forearm, that are split into two distinct compartments; the anterior compartment, which contains the flexors, and the posterior compartment, which contains the extensors.

The forearm muscles in the anterior compartment (Figure 1) are eight and are involved in flexion of wrist and fingers. They also perform pronation, which is the rotation of the palm upside down. They're divided into three layers; superficial muscles, which lie close to the skin; deep muscles, which lie near to the bones (radius and ulnar); and intermediate muscles, which lie between the superficial and deep Forearm muscle.

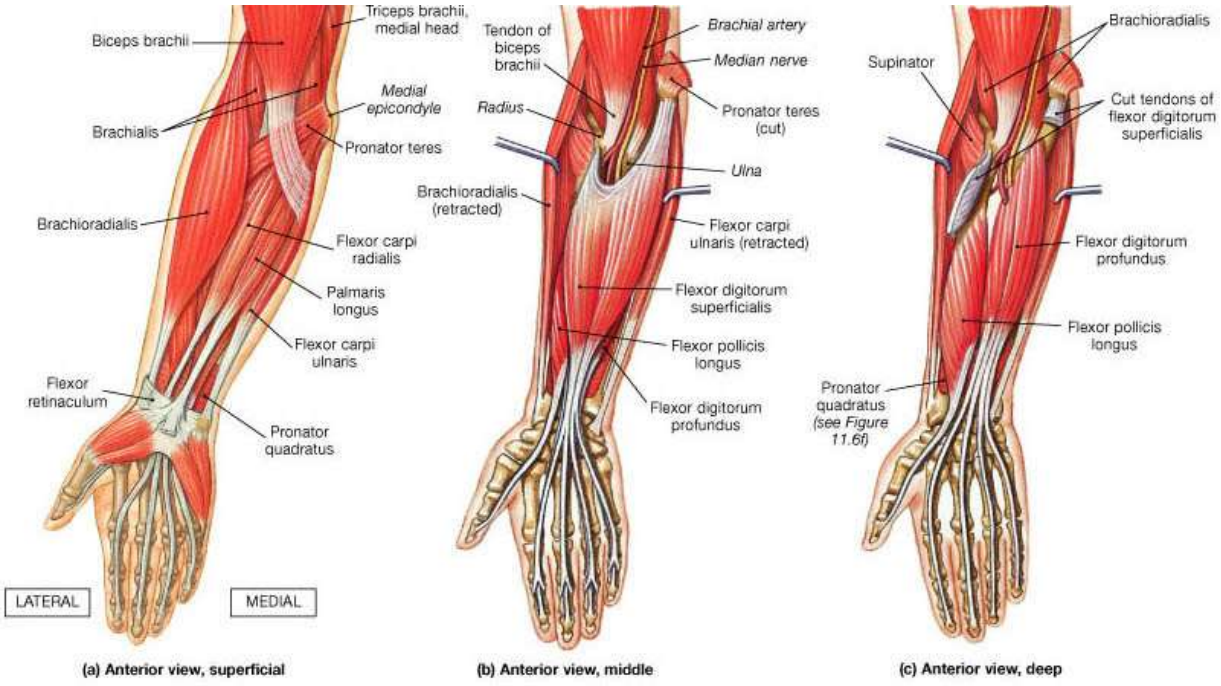

Figure 1: Frontal view of the anterior forearm compartment [26].

The forearm extensors, which are contained in the posterior compartment (Figure 2), are twelve and act to extend the wrist and fingers and are separated into two layers; superficial and deep. While there are only 8 forearm flexor muscles, there are 12 unique forearm extensor muscles, 5 of which originate at the lateral epicondyle of the humerus.

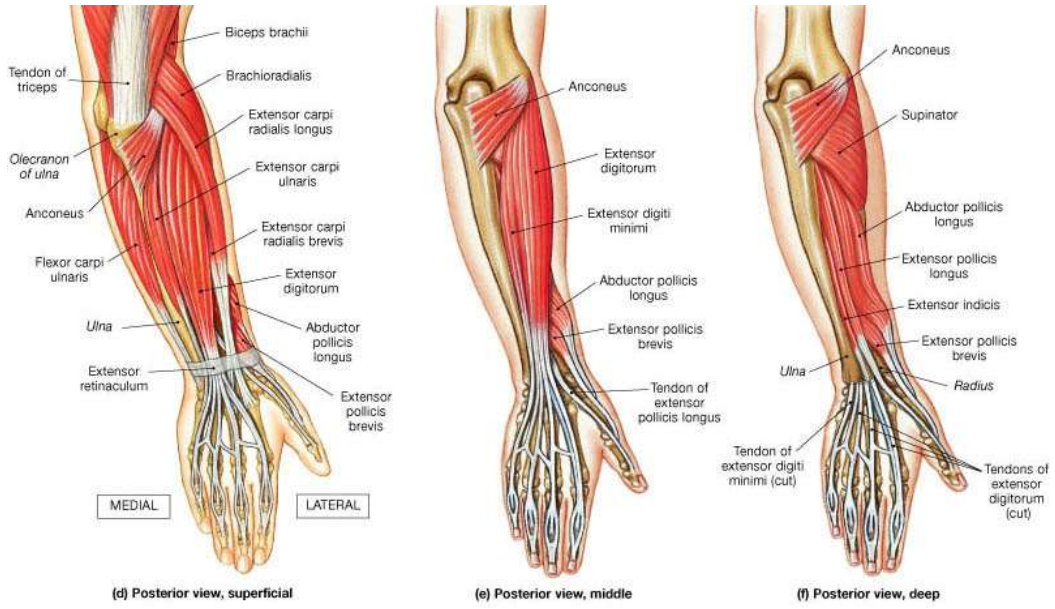

Figure 2: Frontal view of the posterior forearm compartment [26].

2.2 Wrist joint motions

Each of these muscles are involved singularly or in group in different type of task. About the movements around the wrist, which is a joint with three degrees of freedom, the main ones are: flexion, extension, adduction, abduction, supination and pronation.

Flexion (or palmar flexion) at the radioulnar joint is described as the movement in which the palmar aspect of the hand moves towards the anterior compartment of the forearm. Extension (or dorsal flexion) conversely allows the palmar aspect of the hand to move away from the front of the forearm, towards the forearm posterior compartment. Generally, the range of motion for flexion in the radiocarpal joint is about 60°, while for extension it is somewhere around 60° (Figure 3) [27].

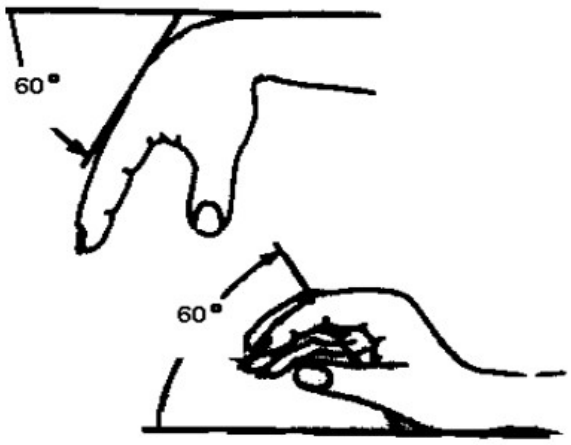

Figure 3: Wrist flexion and extension motion range [27].

The wrist uses a unique form of adduction called ulnar deviation. This describes the outward movement of the hand at the wrist in the direction of the pinky finger. Instead, abduction, also called radial deviation, describes the inward movement of the hand at the wrist in the direction of the thumb. Normal ranges of motion for ulnar deviation and radial deviation are 30° and 20° respectively (Figure 4) [27].

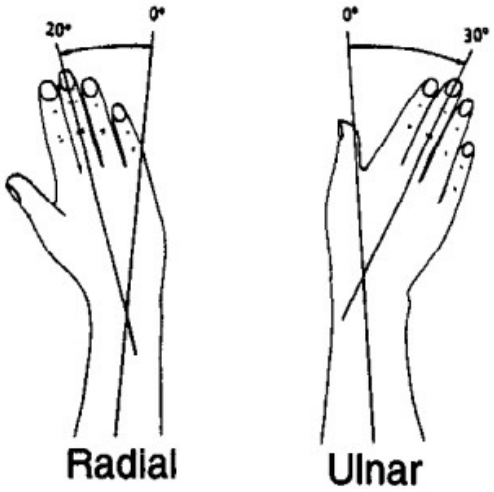

Figure 4: Wrist radial and ulnar deviation (abduction and adduction) motion range [27].

Supination and pronation are movements that occur along the axis of the forearm. More specifically, it's possible to describe these movements referring to the two bones of the forearm: radio and ulna. During supination while ulna remain stable, the radius rotates around it with a clockwise movement, in order to face up forearm and hand palm. Instead, during pronation while ulna remain stable, the radius rotates around it with an anti-clockwise movement, in order to face down forearm and hand palm. Normal ranges of motion for both supination and pronation, are of 80° degrees (Figure 5) [27].

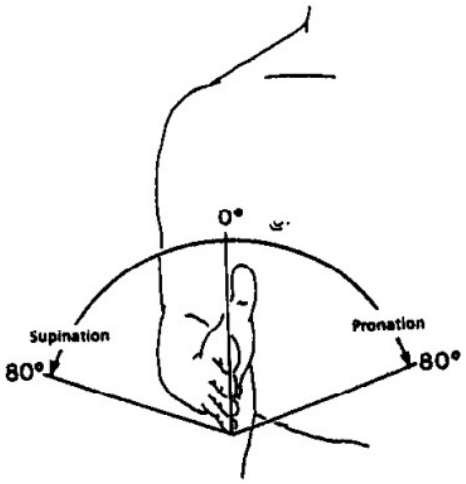

Figure 5: Forearm supination and pronation motion range [26].

2.3 Definition of the experiment

Six healthy subjects, 3 men and 3 women aged between 21 and 50, took part in this experiment. One of them is left-handed, all the others are right-handed. All participants were asked to accomplish two different tasks of wrist motion, sitting in a comfortable position and leaning the arm on the armrest of a chair to not feel fatigued during the task. The first motor task consists of cyclic movement of flexion/extension, while the second one is the cyclic movement of adduction/abduction. Supination and pronation were not taken in consideration. Both the tasks lasted 7 minutes and were divided into two sequential phases:

- During the first three minutes, the subjects were asked to complete five repetitions of flexion/extension (adduction/abduction) followed by three seconds of stop in the resting position, corresponding to a 0° excursion position, repeatedly until the three minutes ran out.
- During the remaining four minutes, the subjects were asked to carry out continuous flexion/extension (adduction/abduction) movements without stop and with a variable range and speed, until the time ran out.

2.4 Hardware and set up

Before starting the wrist motion tasks, the subjects were prepared for the data acquisition. The devices we used are the OYMotion GForcePro+ for the acquisition of the EMG signals, as previously said, and a next generation inertial measurement unit (NGIMU) for the cinematic data acquisition

2.4.1 OYMotion GForcePro

The gForceTM EMG armband is produced by OYMotion. Respecting the idea of wearability, its dimensions and weight are well restrained. The inner diameter varies from a minimum 65 mm to a maximum of 90 mm, thanks to the elastic armband, making it more comfortable depending on the subject who is wearing it. The height and thickness are respectively of 40 mm and 10 mm, resulting not bulky during the motion tasks also due its light weight of just 78g [28].

Figure 6: OYMotion GForcePro+ dimensions [28] .

The armband contains 8 highly sensitive EMG sensors with differential dry electrodes, 9-axis IMU motion sensor, and communicates through Bluetooth BLE 4.2 [28].

Figure 7: OYMotion GForcePro+ principal components [28].

The feature provided by the model we used are:

- Pose data
- Gesture training
- Gesture recognition
- EMG raw data

In this case, we exploited only the last feature and to access the device data, we used a specific software, after connecting the device via Bluetooth to the computer. The gForceDongle, the USB driver of the GForcePro+, communicates wirelessly through Bluetooth with the gForce armband to send commands to and receive data from gForce. Instead, the visualization and acquisition of data was done using the oym8CHWave software (Figure 8), an open-source EMG data manipulation tool for gForcePro/gForcePro+. It displays waveforms according to real time EMG data from gForcePro on 8 different windows, each one related to the signal acquired from one inner electrode of the device [28].

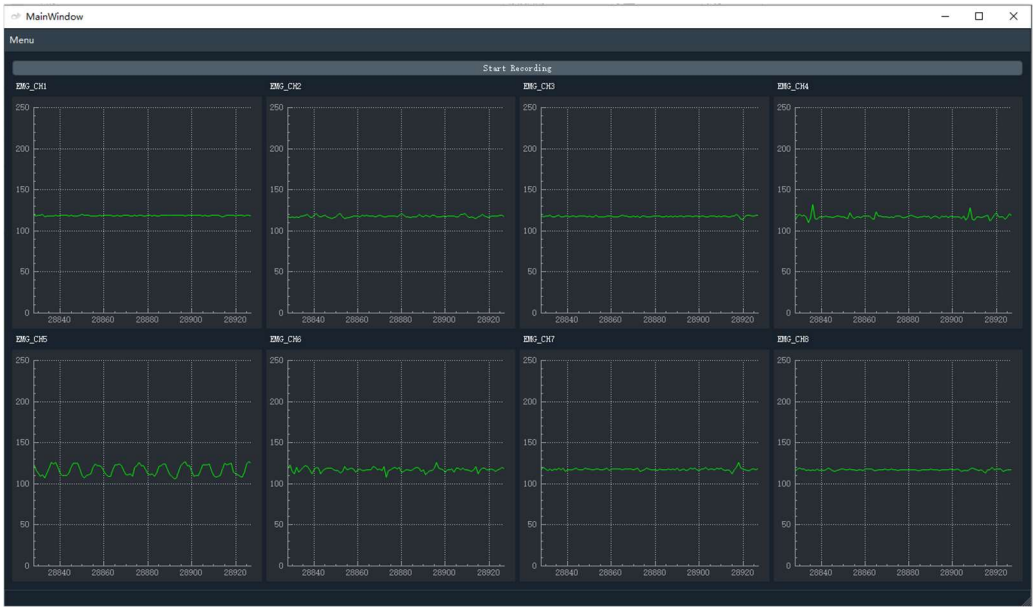

Figure 8: oym8CHWave software for gForcePro+ EMG visualization [29].

After connecting the armband to the computer, the device is paired also to the software. Then it's possible to choose the parameters for data acquisition:

- Sample rate: it ranges from a minimum of 250 Hz to a maximum of 1000 Hz
- Analogue to Digital Conversion (ADC): it allows to choose two different level of quantization, 8 bits (usable with all possible sample rate) and 12 bits (usable with a maximum sample rate of 500 Hz)

Finally, for what concern the positioning, the stainless-steel electrodes on the inner side of the gForce should make good contact with the user's skin otherwise the EMG sensor might not pick up the data properly. To make comparable and consistent acquisition of the data, the wearing position was

standardized across the subject for the experiment: the device was placed at half height of the forearm (Figure 9), in such a way that the USB port was pointing to the palm of the hand.

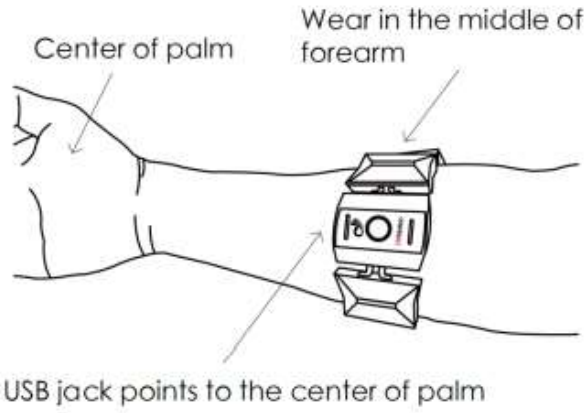

Figure 9: gForcePro+ standardized position used during EMG acquisition [28].

2.4.2 Inertial unit

An inertial measurement unit, or IMU, is an electronic device that measures velocity, orientation and gravitational forces of an object, on which is placed, using a combination of accelerometers and gyroscopes and sometimes also magnetometers. An IMU works by detecting the current acceleration using one or more accelerometers and detects changes in rotational attributes like roll, pitch, yaw thanks to gyroscope measures.

Usually the IMU contains a three-axial accelerometer and three-axial gyroscope [30]. The accelerometers are placed such that their measuring axes are orthogonal to each other. They measure inertial acceleration, also known as G-forces. Three gyroscopes are placed in a similar orthogonal pattern, measuring rotational position in reference to an arbitrarily chosen coordinate system. Recently, more and more manufacturers also include three magnetometers in IMUs. This allows better performance for dynamic orientation calculation in Attitude and heading reference systems which base on the IMU.

The Next Generation IMU (NGIMU), produced by x-io Technologies company, is a compact IMU and data acquisition platform that combines on-board sensors and data processing algorithms with a broad range of communication interfaces to create a versatile platform well suited to both real-time and data-logging applications [31].

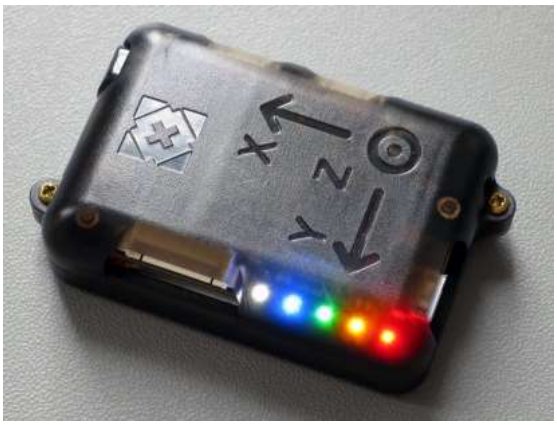

Figure 10: NGIMU box case.

On-board sensors include a triple-axis gyroscope, accelerometer, and magnetometer, as well as barometric pressure sensor, humidity sensor, altitude sensor and temperature sensor. An on-board attitude and heading reference system (AHRS) sensor fusion algorithm combines inertial and magnetic measurements to provide a drift-free measurement of orientation relative to the Earth, and giving as output Quaternion, Rotation Matrix, Euler Angles, Linear Acceleration, Earth Acceleration

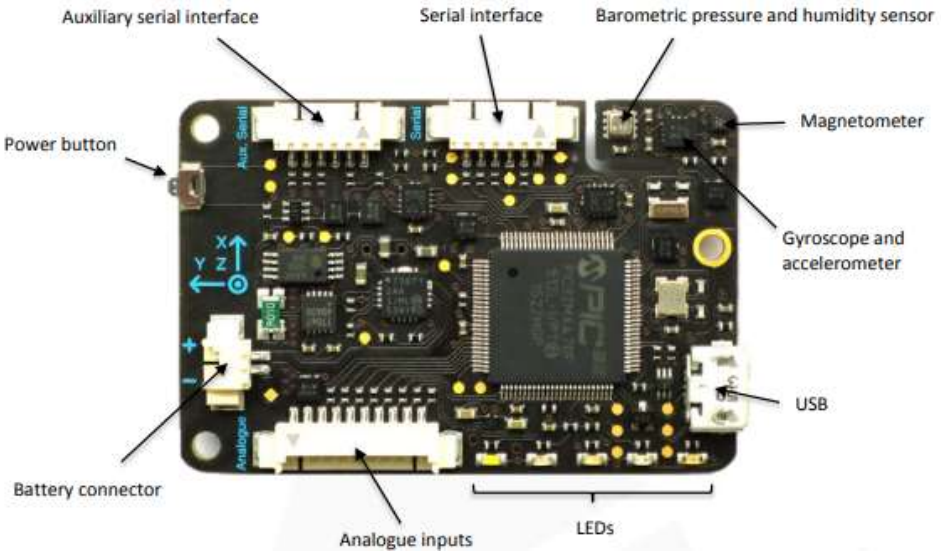

Figure 11: Top view of electronic board of NGIMU [31].

Thanks to its restrained dimensions (56 x 39 x 18 mm with Housing or 50 x 33 x 8 mm Board Only) and light weight (46g With Housing, 10g Board Only) it's possible to measure the inertial characteristics even of little object and, in this case, of short limb segments like the hand.

The data can start to be recorded through a specific software, the NGIMU Gui, after pairing it with the IMU. The NGIMU movement sensor can do real-time communication with a host computer via WiFi [31].

In our study, the NGIMU's output of interest were the quaternion, estimated with a sample rate of 50 Hz, used to reconstruct the wrist motion task in terms of angle variation, around the XYZ axis of the IMU, expressed in radiant. Unit quaternions, known as versors, provide a convenient mathematical notation for representing spatial orientations and rotations of elements in three-dimensional space. Specifically, they encode information about a rotation about an arbitrary axis. When used to represent rotation, unit quaternions are also called rotation quaternions as they represent the 3D rotation group. Compared to rotation matrices, quaternions are more compact, efficient, and numerically stable. Compared to Euler angles, they are simpler to compose [32].

During the experimental protocol considered for this study the IMU was placed on the hand back, of the dominant upper limb of the subject, and fixed using an elastic band to keep the sensor on the back of the hand as still as possible during the motion. The orientation of the sensor on the hand was standardized in such a way like is show in Figure 12.

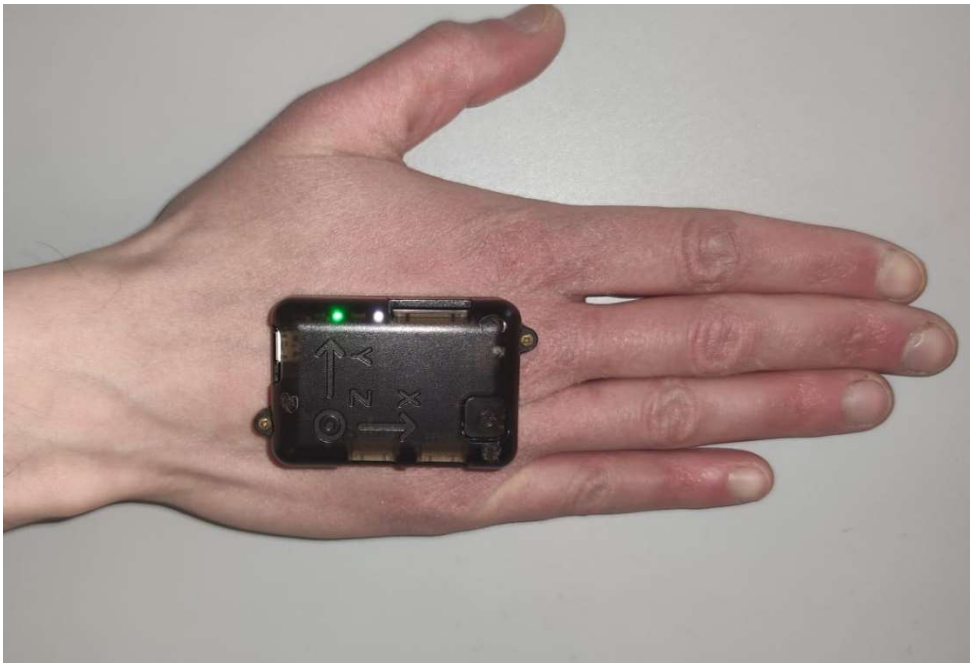

Figure 12: Standardized positioning of NGIMU used during wrist motion acquisition.

- -flexion/extension movements occurred around the Y axis of the IMU
- -adduction/abduction movements occurred around the Z axis of the IMU
- -supination/pronation movements occurred around the X axis of the IMU

The computation of the XYZ angles, starting from the quaternion, was done defining flexion and adduction as positive displacement, while extension and abduction as negative displacement.

2.5 EMG acquisition and preprocessing

The acquisition of EMG signal was done using a sampling frequency of 1000Hz and a quantization level of 8 bits.

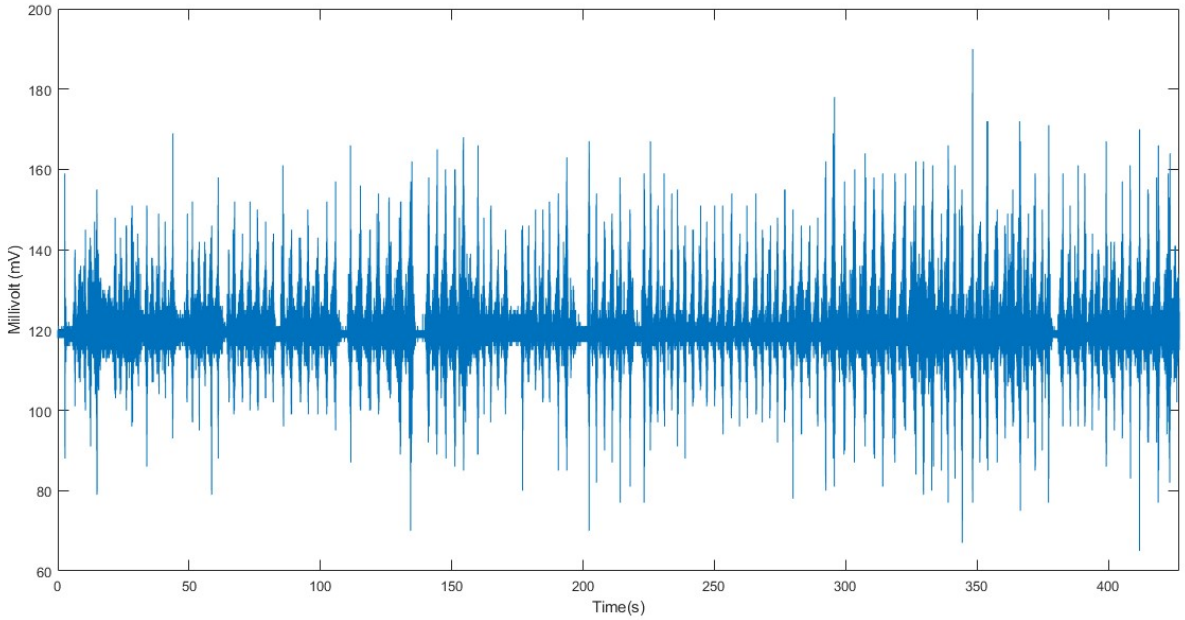

Figure 13: 4th channel Raw EMG signal acquired by Subject 2

The acquisition of EMGs and cinematic data was done simultaneously. Since the acquisition systems for both the devices were different, data were not automatically synchronized. In order to reduce the temporal delay produced by the synchro lack, at the beginning of motion, each subject was asked to accomplish a rapid movement (flexion in the flexion/extension and adduction in adduction/abduction task respectively) followed by 5 seconds of resting at the offset position of 0°. This impulsive displacement causes in the EMGs a spike due to fast contraction of the muscles, while in the cinematic data causes a spike due to the impulsive movement.

The data synchronization was the first step of signal pre-processing, realigning the signals so that the peaks, related to the impulsive displacement corresponded to the same instant of time. Successively we removed the zero-frequency component to obtain zero offset EMG signals. Indeed, the armband introduce a bias in each of acquired signals of about 300 mV. Then, a bandpass second order Butterworth filter with 30 Hz lower cut-off frequency and 450 Hz higher cut-off frequency was applied, since, as we found in literature, this range capture the representative frequency content for this type of signals [24], [25].

2.6 Segmentation of EMG signal

EMG signal is highly variable in nature, and a segmentation approach is required to analyze its random and dynamic pattern. Pre-processed EMG signal is not regarded as a useful input to regression and classification techniques, due to its random nature that makes more difficult the identification of meaningful patterns in the EMG [33]. Therefore, windowing methods are largely adopted to segment and prepare data to further regression. Basically, windowing means sub-dividing the entire signal into small parts, with a proper length, from which features will be extracted. There are mainly two types of windowing methods, which are mostly used in feature extraction: adjacent windowing and overlapping windowing [33]. In the first approach, a window of predefined length is taken at the beginning of the signal, and then shifted forward of the same length of the window. The feature extracted from the portion of the windowed signal include the informative content of more samples that are not shared by adjacent windows. However, this approach of windowing does not generate a dense array of signals and the whole information may be underutilized [34].

Instead, in overlapping window approach, a window of predefined length is chosen and then, starting from the beginning of the signal, its forward shifting is not anymore equal to the original size of the window, but it is less than the original window size, usually expressed as percentage of the window length. In this way, information contained in one window is shared with the adjacent one, creating a signal that makes full use of the available processing power [35]. The choice of window length is a delicate step since the size of the window has a direct relationship with the quality of the extracted features. In general, the greater is the window size, the smoother is the feature obtained, due to the filtering behavior of the window [36]. Indeed, a larger amount of data will result in features with lower statistical variance. On the other hand, large window sizes are much more expensive in terms of computational burden [36]. Hence, the choice of the window size represents a tradeoff between a real time delay and regression performance. Typically, window sizes should be studied according to the specific task that is investigated. However, more recent studies suggested that the window size should optimally be kept between 100-250ms [36], [37].

In the present work, we set the window size to 200ms with an overlap of 20ms (10% of the window dimension). The reasons behind the choice of this overlap size were twice. Firstly, this short forward of the window allowed us to obtain signals with high density of muscle contraction information, resulting in shorter signal containing information related to much longer signal. Secondly, this overlap approach can be seen also as resampling technique, because from the samples belonging to one window, we obtain only one sample: IMU quaternion were acquired with a sampling frequency of 50 Hz, while the EMG signals 1000 Hz. In this way, these latter were 20 times longer with respect to the

cinematic data. Setting the overlap to 20 ms allowed us to obtain signals of the same length. This approach was applied both to extract feature set, used as inputs for machine learning regressors, and to EMG signals used as input for the signal-driven model [24].

2.7 Feature extraction

Selection and extraction of the features is one of the most critical stages in pattern recognition and myoelectric control design. Pattern recognition problems depends almost entirely on the selection of appropriate features [38]. Normally, feeding a regressor with a raw myoelectric signal is impractical due to randomness of the signal, which makes more difficult the pattern recognition task exerted by the regressor. Therefore, the sequence must be mapped into a smaller dimension vector, that is a feature vector [38]. Data features computed over a time window approximate the true value of a feature, with an associated bias and variance. Indeed, in general, features are strongly dependent on the window length and the method of feature extraction. There are three different ways to compute features starting from a general by a signal, they can be computed in the: time-domain, frequency-domain, and time frequency-domain

In the present study, we decided to use the well-known Hudgins' feature set (set of four-time domain features) [39], being used in a considerable number of myoelectric pattern recognition studies, which makes it one of the most valuable set for benchmarking [40], [41]. In addition, inspired by the study of Ali Ameri et al in 2019 [24], we decided to add one frequency domain feature, in order to include frequency spectrum information of muscular contraction.

2.7.1 Time domain features

Time-domain features are the most popular in joint motion estimation because of their computational simplicity, fast implementation and no transformation required [38]. On the other side, time-domain features have the disadvantage that amplitude of signals is strongly influenced by electrode location, the thickness of tissues, the distribution of motor units in muscle fiber, muscle conduction velocities and the detection system used for the acquisition. Amplitude fluctuations and, more in general, a non-stationarity and randomness of the signal, result in changing of statistical properties over time [18]. Moreover, due to their calculations based on EMG signal amplitude values, high interference levels that affect recording acquisition, results in an important drawback, especially for features that are

extracted from energy property [42]. Time-domain features, of Hudgins' set, that we have extracted are listed below:

Mean Absolute Value (MAV) is one of the most used features in EMG signal analysis. This feature is an average of absolute value of the EMG signal amplitude in a segment, which can be defined as:

$$MAV = \frac{1}{N}\sum_{i=1}^{N}|x_i| \quad (1)$$

Waveform Length (WL) is defined as cumulative length of the EMG waveform over the time window. It is computed as:

$$WL = \sum_{i=1}^{N-1}|x_{i+1} - x_i| \quad (2)$$

Zero Crossing (ZC) describes the number of times that amplitude values of the EMG signal cross zero amplitude level:

$$ZC = \sum_{i=1}^{N-1}[sgn(x_i \cdot x_{i+1}) \cap |x_i - x_{i+1}| \geq threshold] \quad (3)$$

$$sgn(x) = \begin{cases} 1 & if\ x \geq threshold \\ 0 & if\ x < threshold \end{cases}$$

Slope Sign Change (SSC) is the number of times that slope of the EMG signal changes sign. The number of changes between the positive and negative slopes among three sequential segments is performed with a threshold function [18]. It is expressed as:

$$SSC = \sum_{i=2}^{N-1} f[(x_i - x_{i-1}) \cdot (x_i + x_{i-1})] \quad (4)$$

$$f(x) = \begin{cases} 1 & if\ x \geq threshold \\ 0 & if\ x < threshold \end{cases}$$

2.7.2 Frequency domain feature

Frequency domain analysis is used for EMG evaluation; the spectrum of EMG signal contains useful information about contraction force (in a time-invariant manner) and so it can be exploited for pattern recognition problems [43]. Indeed, the spectrum is influenced mainly by two factors: the firing rate of a recruited muscle unit in the low frequency range (below 40 Hz), and the morphology of the action potential travelling along a muscle fiber in a high-frequency range (above 40 Hz) [44]. The only frequency domain feature considered in this study is shown below

Mean Frequency (MNF) is an average frequency which is calculated as sum of product of the EMG power spectrum and the frequency divided by total sum of the spectrum intensity. It is calculated as:

$$MNF = \frac{\sum_{j=1}^{M} f_j \cdot P_j}{\sum_{j=1}^{M} P_j} \quad (5)$$

where f_j is frequency of the spectrum at frequency bin j, P_j is the EMG power spectrum at frequency bin j, and M is length of the frequency bin.

2.8 Data set splitting for training and testing phase

Feature sets are under the form of matrices that contain all the numeric values of features, appended with a target array. These labels are necessary to the algorithms during training phase, when the machine has to learn relationships between available data and target signal. Moreover, target values are necessary to check the validity of degree of learning of the machine in validation phase, and to test the final regression performance. For this reason, algorithm should learn a relationship that correctly generalizes to new examples beyond the training dataset. This purpose motivates the use of cross-validation to estimate the performance of the model when making predictions on data not used during training.

All the trained models are validated through a holdout cross validation. This latter is a very popular technique used to validate model predictions, when large data set are available and low training time are requested. Holdout cross validation randomly divides the dataset into two groups, or folds. The first fold is conserved for validation, and it's composed by a number of randomly chosen samples, equal to a selectable percentage of the total training set. The remaining portion is used to train the model. This approach is used for trying to reduce the overfitting of data. Overfitting refers to a model

that predicts over the training data too well. This phenomenon happens when a model learns the detail and noise in the training data to the extent that it negatively impacts the performance of the model on new data. This means that the noise or random fluctuations in the training data is picked up and learned as right concept by the model. The problem is that these relationships do not apply to new data and deny the trained model to generalize over new inputs.

In this study we divided the data in the following manner: the last 10% of the whole data set was used in testing phase, while the initial 90% was used to train the regression models. More precisely, the training data set was ulteriorly divided into a randomly chosen 30% for the holdout cross validation, while the remaining portion was actually used for the training.

2.9 Regression algorithms

As previously said, in this study we approached the problem of wrist motion estimation using two different methods: features-driven and signal-driven. As a features-driven approach, we used the Random Forest (RF) algorithm. While, for signal-driven approach, a Convolutional Neural Network (CNN) was proposed and trained with the raw EMG signal.

2.9.1 Random Forest

RF is a supervised machine learning algorithm that is constructed from decision tree algorithms. It utilizes ensemble learning, which is a technique that exploits the combination of many regressors to provide precise solutions to complex problems. A random forest algorithm is basically an ensemble of many decision trees. It predicts by taking in account all the outputs from various trees that compounds the forest [45]. A decision tree consists of split nodes and leaf nodes, as shown in Figure below.

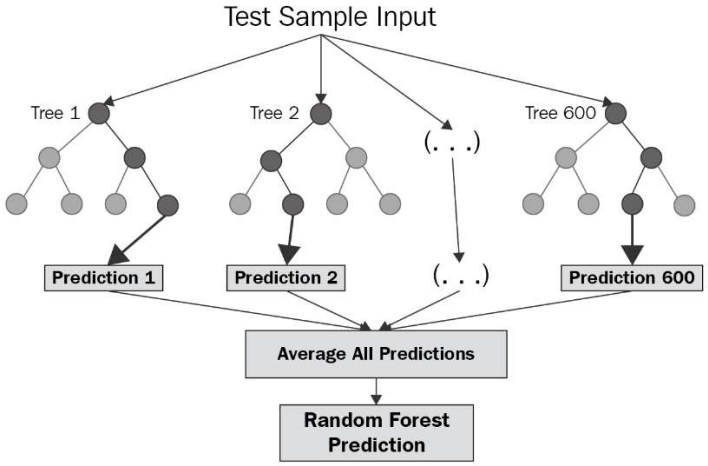

Figure 14: Visual schematization of Random Forest Algorithm structure [46].

Each split node performs a split decision and routes a data sample x to the left child node or to the right child node. To let the tree, know where to address the decision, a set of rules is necessary. Rules are under the form of numerical thresholds. The data sample x is routed to the left child node if the value of feature of x is smaller than a threshold and to the right child node otherwise. All leaf nodes store votes for the value of the target. Starting at the root node, the data is recursively split into subsets. In each step the best split is determined according to specific criteria, like Gini index or entropy level, determining the information gain reached at the leaves of the tree [45]. Regression in random forests employs an ensemble methodology to attain the outcome. The training data is fed to train various decision trees. This dataset consists of observations and features that will be selected randomly during the splitting of nodes. In regression problems, the final output of the random forest algorithm is given by the average of each decision tree output.

2.9.2 Convolutional Neural Network

CNN is a DL technique, which is a method used to create models that mimic the functionality of human brain. These models are made up of several layers which can extract features from the data; each layer of these neural networks, starting from the left-most layer to the rightmost layer, extract a low-level feature like edge and subsequently make predictions accurately. DL methods use Neural Networks, so, they are often referred to as Deep Neural Networks.

CNN usually consists of two operations: convolution and pooling. Multiple filters are used for the convolutions to extract edges, corners, or other high-level features from an image automatically. Then, a pooling layer follows, such as max pooling, which selects the largest number in a box, which aims at keeping the most significant features of the original picture while decreasing the number of input dimensions. After undergoing a few layers of convolution and pooling, the abstract features extracted by the CNN will be used for tasks such as classification or regression through several fully connected layers and an output layer. CNN is not the same as multilayer perceptron, which is composed by fully connected layers, where every neuron connects with all the neurons in the next layer. CNN has only local connections among the neurons and adjacent layers, instead. It also shares the same parameters for different parts of the image. These characteristics save on the number of parameters and thus promote more efficient training. By adjusting the network structures, better prediction results can be accomplished. CNN is of vital importance for EMG decoding using deep learning methods. Most research decodes human intention with an “EMG image” using a CNN. The features learned by the CNN have resulted in state-of-the-art performance for EMG recognition [23].

The CNN-based model used in this study was prepared as follows. The model was applied on raw EMG data. First, each EMG segment of 1600 sample (200 ms windows for each of the eight channels of acquisition, aligned to form a unique vector) was arranged to form a 40x40 matrix image. Then the next images are obtained analogously, by aligning windows from each EMG signal shifted 20ms forward.

The layers composing this structure were:

- Image input layer: inputs 2-D images to a network and applies data normalization.
- Convolutional layer: applies sliding convolutional filters to 2-D input. The layer convolves the input by moving the filters along the input vertically and horizontally and computing the dot product of the weights and the input, and then adding a bias term. Depending on the number of applied filters, the same number of activation map will be generated.
- Batch Normalization Layer: normalizes a mini batch of data (small set of the validation data) across all observations for each channel independently, to speed up training of the convolutional neural network and reduce the sensitivity to network initialization. In our analysis, the batch normalization layers were inserted between convolutional layers and nonlinearities.
- Function activation layer: conduct nonlinear transformations. Nonlinear activation functions are important because, otherwise, the network would be a linear predictor, without the ability to learn nonlinear features. An example of function activation layers is rectified linear unit (RElu), sigmoid or hyperbolic tangent functions. In our study the RElu activation function was used, which is a non-linear function that gives output only if the input is positive, otherwise, the output will be zero. It is often used because it does not saturate, hence the network can train much faster, with similar accuracy.
- Pooling layer: performs down sampling by dividing the input into rectangular pooling regions, then computing the average values of each region.
- Fully connected layer: multiplies the input by a weight matrix and then adds a bias vector, performing high level resoning.
- Regressor layer: determines how training penalizes the error between the predicted and true values, for classification or regression problems.

The proposed CNN had 32 layers consisting of an input layer, eight convolution layers, each followed by a normalization and RElu layers, five average pooling layers, a fully connected layer, and a regression layer. The eight convolution layers had 16, 16, 64, 64, 64, 64, 16, 16 filters, respectively,

where all filters were 3x3. The input matrices were zero-padded before convolution, in order to maintain coherence in data dimensionality. Average pooling was conducted on 2x2 areas, which was slipped laterally and vertically of two samples.

The model was trained with a Stochastic Gradient Descent (SGD) method which is an iterative method that updates the network parameters (weights and biases) to minimize the loss function by taking small steps at each iteration in the direction of the negative gradient of the loss. More specifically, the stochastic gradient descent algorithm evaluates the gradient and updates the parameters using a subset of the training data called mini batch, which in our study was set to 128, being a good compromise between regression performances and training time [24], [11].

2.9.3 Regression performance metrics

Once the feature-based and data-driven models were trained, we proceeded with testing phase using the 10% of the acquired signals as testing data set. The predicted outcomes of the regressors were lowpass filtered using a third order Butterworth filter with a cutoff frequency of 1 Hz, as Almeri et al. did in their work of 2019 [24].

In order to evaluate the performance and make a consistent comparison between the two methods we used; the following statistical coefficient were computed:

- R-squared (R^2): it is an important statistical measure which is a regression coefficient that represents the proportion of the difference or variance in statistical terms for a dependent variable which can be explained by an independent variable or variables. it determines how well data will fit the regression model.

$$R^2 = 1 - \frac{SSE}{SST} \quad (12)$$

Where SSE being the sum of squared error, and SST the sum of squared total

$$SSE = \sum_{i=1}^{N} (y_{est}(i) - y_{real}(i))^2 \quad (13)$$

$$SST = \sum_{i=1}^{N} (y_{real}(i) - y_{mean})^2 \quad (14)$$

With y_{real} that is the acquired cinematic data and y_{est} the output of prediction.

- Root Mean Square Error (RMSE): The term root mean square error (RMSE) is the square root of mean squared error (MSE). Unless the relationship or correlation is perfect, the predicted values are more or less different from the actual observations. These differences are prediction errors or residuals. RMSE measures these residuals by the vertical distances between the actual values and the regression line. Large distances are indicative of large errors.

$$RMSE = \sqrt{\frac{\sum_{i=1}^{N}(y_{real}(i) - y_{est}(i))^2}{N}} \quad (15)$$

Where N indicates the number of samples of the signals.

Root Mean Square Difference (RMSD): It's very similar to the RMSE coefficient. This latter one indicates the mean error between the measured and estimated signal, expressed, in our study, in degrees. The root mean square difference represents this same error but is expressed in percentage.

$$RMSD = \sqrt{\frac{\sum_{i=1}^{N}(y_{real}(i) - y_{est}(i))^2}{\sum_{i=1}^{N}(y_{real}(i))^2}} \quad (16)$$

3 Results

This section contains all the results carried out from our experiments, divided into two sections: Flexion/Extension task results and Adduction/Abduction task results. Firstly, are reported the 8 channel EMG signals acquired using the OYMotion GForcePro+ and at last the corresponding joint motion signal.

Then, it will be shown the evaluation and consideration obtained using the Random Forest algorithm and the Convolutional Neural Network, during both the training and testing phase. In order to have a general overview about the performance of the RF and CNN models we took in consideration the mean value of the statistical coefficients, previously named, computed for each subject.

3.1 Flexion/extension task results

The first figure (Figure 14) shows random picked ten seconds window of the recorded 8 channel EMG signals acquired through OYMotion GForcePro+ from the Subject 2, during the flexion/extension task which is reported on the bottom of the figure. Then, in Table 1 are reported the mean R^2, RMSE and RMSD values, with their corresponding standard deviation, computed on the outputs obtained using the training data set (including the validation data set), while Table 2 contains results obtained using the testing data set. Then, in Figure 15 and Figure 16 are reported the fitting curves (related to Subject 2), obtained using the Convolutional Neural Network and the Random Forest, respectively of wrist flexion/extension motion after the training phase and testing phase.

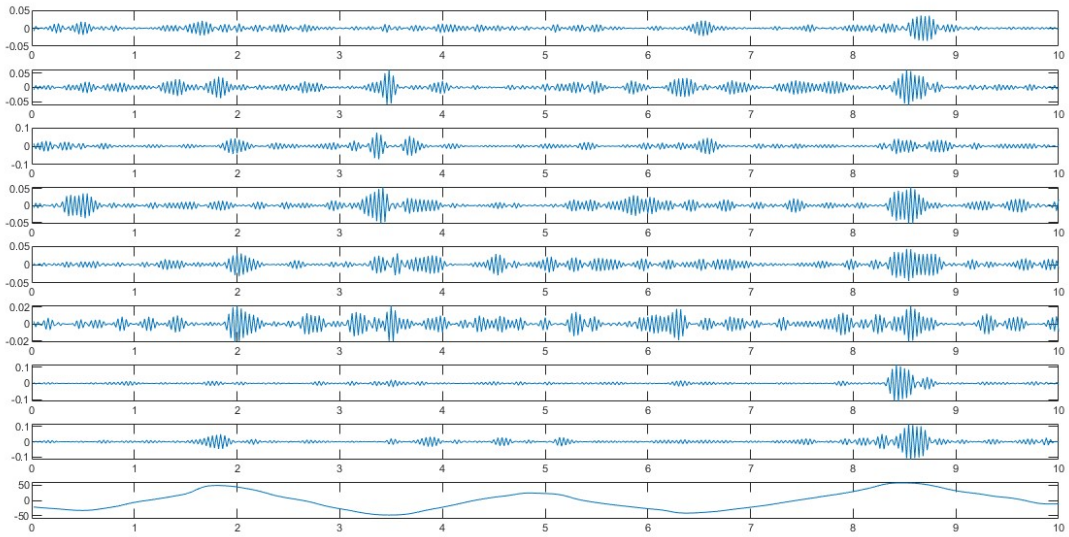

Figure 14: 8 channel EMG signals acquired through OYMotion GForcePro+ from the Subject 2 and corresponding flexion/extension signal

Table 1: Statistical coefficient computed for flexion/extension task estimation in training phase

	R^2 (%)	RMSD (%)	RMSE (°)
RF	88 ± 6	32 ± 8	9 ± 2.5
CNN	95 ± 1	22 ± 4	6 ± 3.6

Table 2: Statistical coefficient computed for flexion/extension task estimation in testing phase

	R^2 (%)	RMSD (%)	RMSE (°)
RF	73 ± 12	47 ± 8	16 ± 3.8
CNN	83 ± 8	36 ± 6	12 ± 3.6

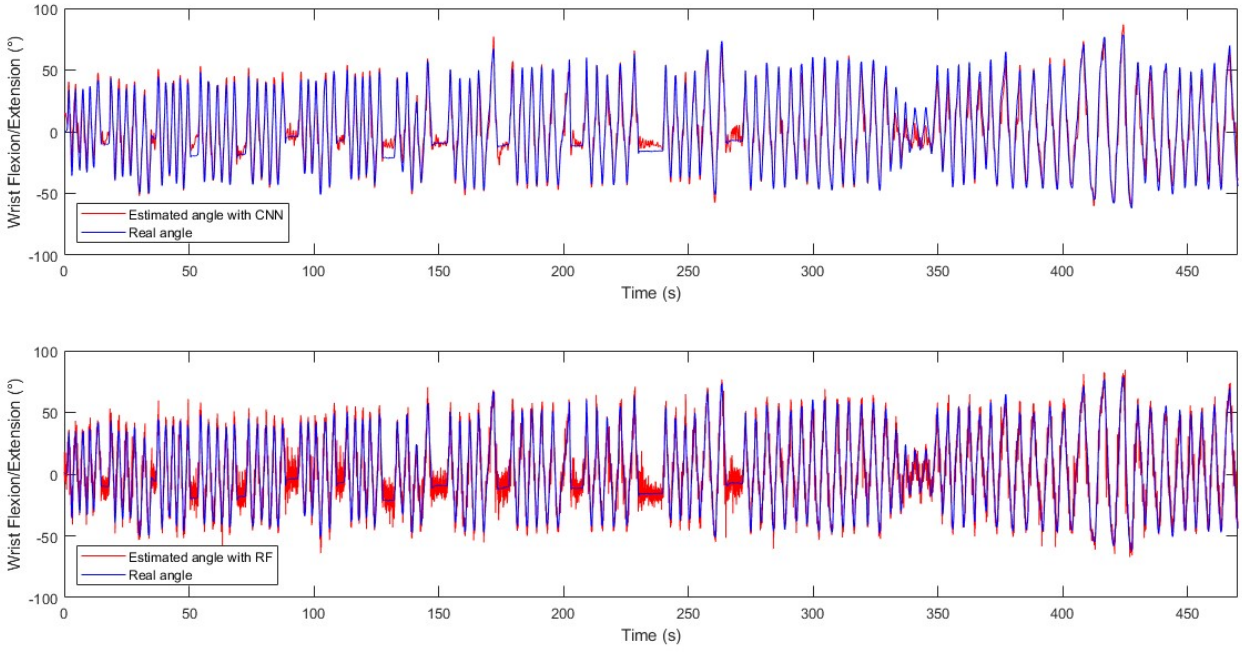

Figure 15: Subject 2 wrist flexion/extension motion estimation during training phase, using RF and CNN.

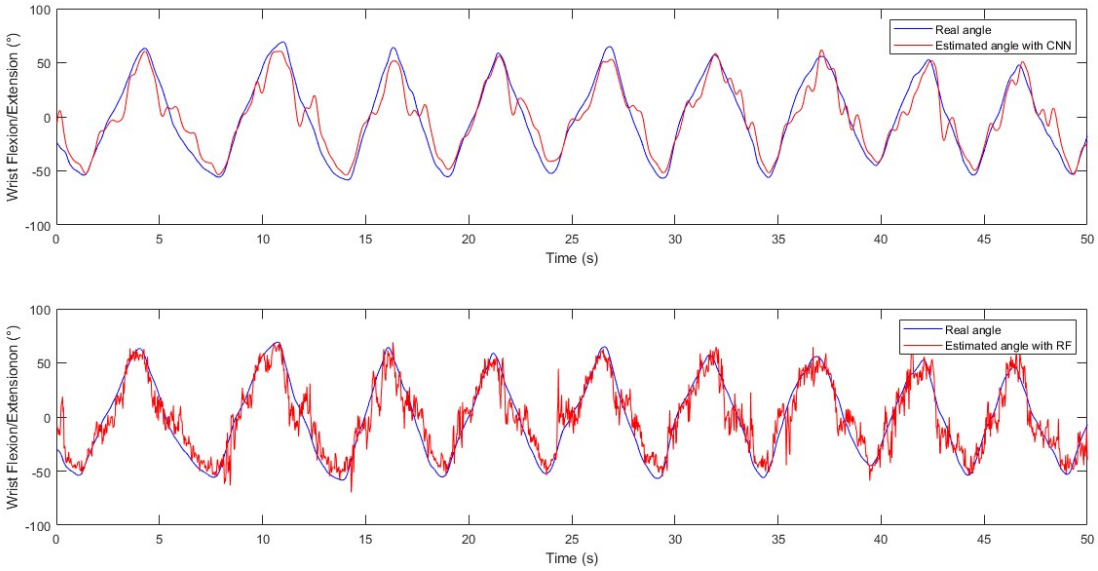

Figure 16: Subject 2 wrist flexion/extension motion estimation during testing phase, using RF and CNN.

3.2 Adduction/abduction task results

Analogously to previous paragraph the first figure (Figure 17), shows random picked ten seconds window of the recorded 8 channel EMG signals acquired through OYMotion GForcePro+ from the Subject 2, during the adduction/abduction task, which is reported on the bottom of the figure. Table 3 and Table 4 reports R^2, RMSE and RMSD mean values, with their corresponding standard deviation, computed, respectively, after the training and testing phase. Figure 18 and Figure 19 report the adduction/abduction wrist motion fitting curves, obtained respectively after the training and testing phases.

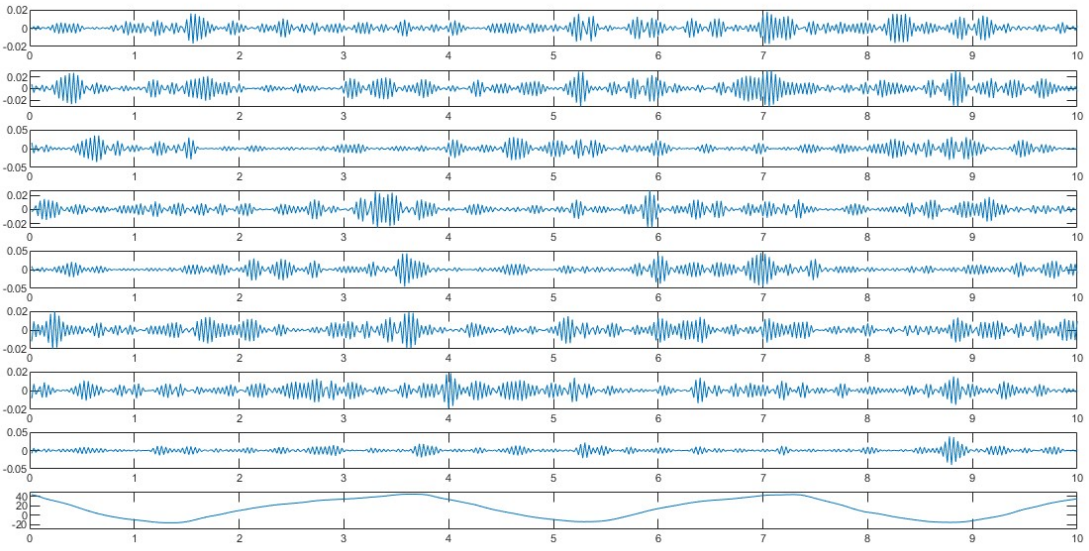

Figure 17: 8 channel EMG signals acquired through OYMotion GForcePro+ from the Subject 2 and corresponding adduction/abduction signal.

Table 3: Statistical coefficient computed for adduction/abduction task estimation in training phase

	R^2 (%)	RMSD (%)	RMSE (°)
RF	85 ± 9	32 ± 11	8 ± 3.0
CNN	93 ± 2	22 ± 5	6 ± 3.6

Table 4: Statistical coefficient computed for adduction/abduction task estimation in testing phase

	R^2 (%)	RMSD (%)	RMSE (°)
RF	78 ± 10	38 ± 9	10 ± 1.8
CNN	82 ± 14	36 ± 15	9 ± 1.7

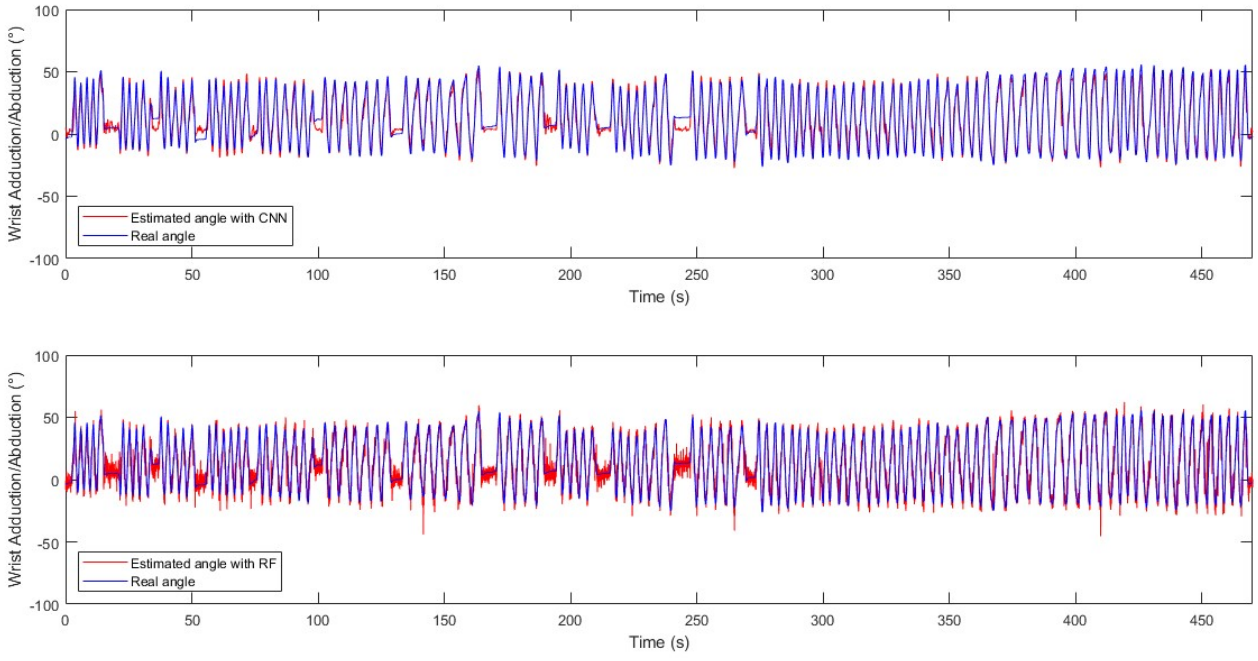

Figure 18: Subject 2 wrist adduction/abduction motion estimation during training phase, using RF and CNN.

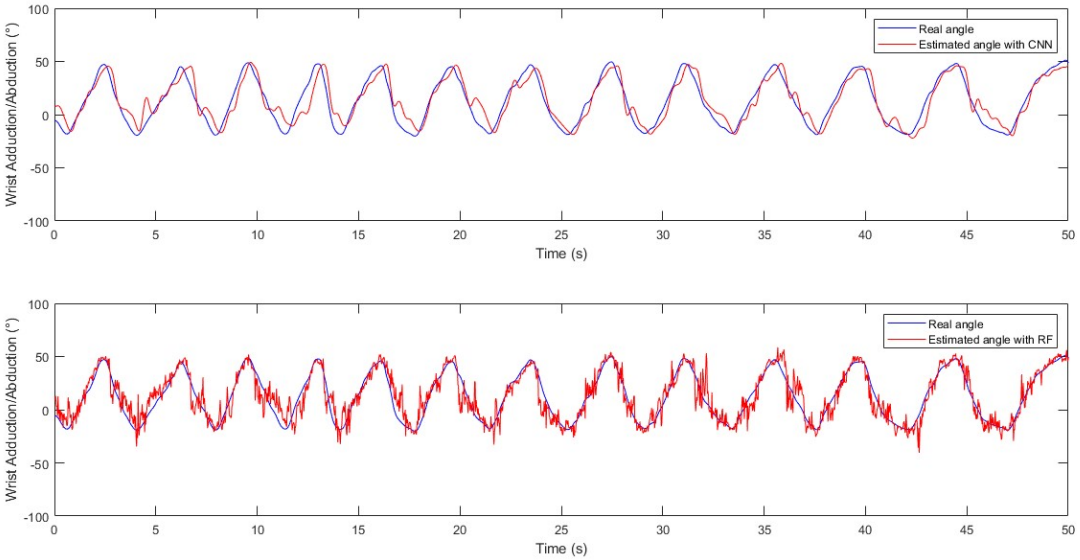

Figure 19: Subject 2 wrist adduction/abduction motion estimation during training phase, using RF and CNN.

4 Discussion and conclusion

Results are discussed starting from the Random Forest and Convolution neural network performance comparison in the training phase.

From Figure 15 and Figure 18, it's possible to have a visual inspection of the goodness in the fitting behavior of the two models. Despite the wide motion range of approximately 100°, with a maximum excursion of 50° in flexion and extension, both the models were able to capture the dynamic of the kinematic signal. Indeed, as reported, in Table 1, the average regression coefficients are very high (88% of fitting using RF and 95% using CNN) and reflect what can be appreciated visually. Moreover, the reported mean RMSE are also very good; on average the RF and CNN has a mean error, respectively, of just 9° and 6° which, over a maximum range of 100°present less than 10% of the real measure. However, the average RMSD gives a clearer idea of the amount of error in the two different estimations. Taking in consideration that predictions are considered excellent if the coefficient of regression is greater than 90% and the RMSD is smaller than 15% [22], the overall performance of the Convolutional Neural Network was better, in training phase, (R^2=95%, RMSD=22%) and outperformed the Random Forest regressor (R^2=88%, RMSD=32%). Indeed, this last one, despite being able to capture the wrist motion dynamics, had fitting curve (Figure 15), that shows higher frequency oscillation around the kinematic signal. More in details, the worst fitting was in correspondence of the resting phase (present in the first half of the signal) during which the subject 2 maintained the wrist in off-set position. Instead, the CNN appeared to be able of smoother and less noisy estimations. For what concern the adduction/abduction task, it's possible to make the same consideration and evaluation since the results reported in Table 3 are almost identical to those reported in table 1: CNN still had better training performance with more accurate output with respect the RF.

However, the most important outcomes are those relative to testing phase because they reflect the ability of a trained regression model to generalize and predict data that it did not see before. Starting from the task of flexion/extension and relying just on a visual inspection, it's possible to say that trained CNN captured almost perfectly the dynamic of the wrist motion (Figure 16). However, the average evaluation coefficient computed (R^2=83%, RMSD=36%, RMSE=12°) (Table 2), despite still being good, are slightly worst with respect those obtained in training phase (Table 1), due to the presence of ripples, small oscillations, around the real cinematic signal (Figure 16). For what concern the prediction of the trained RF model and the corresponding statistical coefficient (R^2=73%, RMSD=47%, RMSE=16°), instead, they appeared to be worse than both the results obtained by the trained CNN model, in testing, and the RF in training phase. Also in this case, the reason behind these

results can be easily grasped by a quick visual inspection of the Figure 16: despite being able to follow the general wrist motion pattern for the entirety of the signal, the trained RF fitting curve is characterized by high frequency oscillation, oscillating around the curve of the real wrist motion angle, leading to a decrease in estimation parameters.

Regarding the adduction/abduction wrist task, very similar results, with respect to the previous task, were obtained when using the CNN: the trained neural network predicted almost perfectly the joint motion (Figure 19), barring the same small ripple present also in the previous estimation of flexion/extension motion (Figure 16). Indeed, the evaluation coefficient computed in this case (R^2=82%, RMSD=36%, RMSE=9°) were identical to those of the first task, with just a small difference in average degree error of 3°. Instead, regarding the trained RF model, a better prediction performance was reached with respect to the estimation of flexion/extension task motion. Despite the fitting curve (Figure 19) was still characterized by high frequency oscillations occurring around the real cinematic signal, making difficult a visual comparison between the two task, prediction coefficient (R^2=78%, RMSD=38%, RMSE=10°), reported in Table 4, were more similar to those obtained in RF training phase (R^2=85%, RMSD=32%, RMSE=8°), reported in Table 3, probably due to less wide range motion task: 50° in adduction/abduction against 100° in flexion/extension.

In general, the signal-driven approach allowed to reach better results with respect to a feature-based method, starting in both the case from the same pre-processed EMG signals, acquired during the wrist motion tasks (Figure 14 and 17). The lower performances of the feature-driven model could be explained in two different ways. Firstly, one reason could be the choice of the features that were extracted from the EMG signals and then used for training the model. There are many different types of features that could be used to obtain the best regressor configuration [18]. In this analysis, the Hudgins' set was used because it represents one of the most used feature set, that many studies exploit for regression and classification purposes, but from the present results, it appeared to be not enough for performing a continuous estimation of wrist joint motion. This leads to the conclusion that a more accurate feature selection must be done, in order to choose the best features that could be the most significant in a study of this type. On the contrary, using a signal-driven approach, it's possible to overcome these drawbacks, since the EMG signal can be given all together as input to the neural network, just after a fast rearrangement of the EMG data into a matrix configuration.
The second reason for the low performance it's due to the usage of the wearable device. Indeed, by using standard surface electrodes, it's possible to place them is such a way that they can register the EMG signal related to one single muscle. There are studies in literature that proposed electrodes

placement configuration that can be exploited to obtain EMG acquisitions that are the most possible related to single muscles activations [47]. In this way, each recording is characterized by the contraction and relaxation of a specific muscle, meaning that the features will contain very discriminative information, allowing the feature-based model to reach better prediction performances. However, using a wearable device, in this case the OYMotion GForcePro+, the surface electrodes, along the inner surface of the armband, are fixed with a fixed distance between them. This means that once wore, depending also on the dimension of the surface electrodes, their positions won't be as located as whether single electrodes are used. This results in a positioning where electrodes could record the activation of undesired muscles, resulting in acquisition of EMG signals that could be poorly synchronized with specific kinetic signal, as shown in Figure 14 and Figure 17. Computing features from these types of signals could affect the correct training of a feature-based regressor. Indeed, the information carried by these features have less discriminative power because they reflect the activation of more muscles, that could also contract and relax with different timing. Therefore, this type of devices could be easier to use when using a signal-driven model that, as said before, can be trained using the totality of the EMG acquisition without any sophisticated transformation, since it uses all the spatial information acquired to extract the most possible discriminative features. All these reasons could be a possible explanation for the fact that, in a set up including a wearable device, the Convolution Neural Network, a feature less method, guaranteed a better performance with respect to a feature-based approach.

Moreover, making a comparison with results found in literature, in research that had a similar approach, it was possible to consider the outcomes of this study promising also for what concern the usage of a wearable device instead of surface electrode, at least in a signal-driven approach. In 2014, Hahne et al. used a high density 192 channel grid to acquire EMG signal, from the forearm, successively used in a feature-based model to estimate a single DoF wrist movement, with a maximum value of fitting equal to 80% [25]. In 2015 El-Khoury et al. used 7 surface electrodes placed on thickest part of the forearm to acquire EMG signal successively used in a feature-based model for the estimation of 2 DoF wrist movement, ending with a maximum fitting value of 72% [20]. In 2019 Bao et al. used 12 bipolar surface electrodes to acquire EMG signals from the forearm. In this study five different feature-based model were compared with one signal-driven model. This last one had the best performance with a fitting of the 84% [11]. The results obtained in this study were very similar to the just previously illustrated, leading to the idea that the implementation of wearable devices in experiments of continuous joint motion estimation could be an optimal alternative to the usage of standard surface electrode.

5 Bibliography

[1] F. Cordella *et al.*, “Literature review on needs of upper limb prosthesis users,” *Frontiers in Neuroscience*, vol. 10, no. MAY. Frontiers Media S.A., 2016. doi: 10.3389/fnins.2016.00209.

[2] P. Fitzgibbons and G. Medvedev, “Functional and Clinical Outcomes of Upper Extremity Amputation,” *Journal of the American Academy of Orthopaedic Surgeons*, vol. 23, no. 12. Lippincott Williams and Wilkins, pp. 751–760, Dec. 01, 2015. doi: 10.5435/JAAOS-D-14-00302.

[3] Z. O. Khokhar, Z. G. Xiao, and C. Menon, “Surface EMG pattern recognition for real-time control of a wrist exoskeleton,” 2010. [Online]. Available: http://www.biomedical-engineering-online.com/content/9/1/41

[4] A. Ziai and C. Menon, “Comparison of regression models for estimation of isometric wrist joint torques using surface electromyography,” 2011. [Online]. Available: http://www.jneuroengrehab.com/content/8/1/56

[5] O. Fukuda, T. Tsuji, M. Kaneko, and A. Otsuka, “A human-assisting manipulator teleoperated by EMG signals and arm motions,” *IEEE Transactions on Robotics and Automation*, vol. 19, no. 2, pp. 210–222, Apr. 2003, doi: 10.1109/TRA.2003.808873.

[6] P. Shenoy, K. J. Miller, B. Crawford, and R. P. N. Rao, “Online electromyographic control of a robotic prosthesis,” *IEEE Transactions on Biomedical Engineering*, vol. 55, no. 3, pp. 1128–1135, Mar. 2008, doi: 10.1109/TBME.2007.909536.

[7] F. Sebelius, M. Axelsson, N. Danielsen, J. Schouenborg, and T. Laurell, “Real-time control of a virtual hand,” IOS Press, 2005.

[8] D. Nishikawa, W. Yu, H. Yokoi, and Y. Kakazu, “EMG Prosthetic Hand Controller using Real-time Learning Method.”

[9] K. Kita, R. Kato, H. Yokoi, and T. Arai, “Development of Autonomous Assistive Devices-Analysis of change of human motion patterns.”

[10] C. Murray, *Amputation, prosthesis use, and phantom limb pain: An interdisciplinary perspective*. Springer New York, 2010. doi: 10.1007/978-0-387-87462-3.

[11] Tianzhe Bao, Ali Zaidi, Shengquan Xie, and Zhiqiang Zhang, *Surface-EMG based Wrist Kinematics Estimation using Convolutional Neural Network*.

[12] T. S. Buchanan, D. G. Lloyd, K. Manal, and T. F. Besier, “Neuromusculoskeletal Modeling: Estimation of Muscle Forces and Joint Moments and Movements From Measurements of Neural Command,” 2004.

[13] Q. C. Ding, A. B. Xiong, X. G. Zhao, and J. D. Han, “A novel EMG-driven state space model for the estimation of continuous joint movements,” in *Conference Proceedings - IEEE International Conference on Systems, Man and Cybernetics*, 2011, pp. 2891–2897. doi: 10.1109/ICSMC.2011.6084104.

[14] D. L. Crouch and H. Huang, “Lumped-parameter electromyogram-driven musculoskeletal hand model: A potential platform for real-time prosthesis control,” *Journal of Biomechanics*, vol. 49, no. 16, pp. 3901–3907, Dec. 2016, doi: 10.1016/j.jbiomech.2016.10.035.

[15] Y. Zhao, Z. Zhang, Z. Li, Z. Yang, A. A. Dehghani-Sanij, and S. Xie, “An EMG-Driven Musculoskeletal Model for Estimating Continuous Wrist Motion,” *IEEE Transactions on Neural Systems and Rehabilitation Engineering*, vol. 28, no. 12, pp. 3113–3120, Dec. 2020, doi: 10.1109/TNSRE.2020.3038051.

[16] M. Sartori, D. G. Llyod, and D. Farina, “Neural data-driven musculoskeletal modeling for personalized neurorehabilitation technologies,” *IEEE Transactions on Biomedical Engineering*, vol. 63, no. 5, pp. 879–893, May 2016, doi: 10.1109/TBME.2016.2538296.

[17] M. Zardoshti-Kermani, B. C. Wheeler, K. Badie, and R. M. Hashemi, “Feature Evaluation for Movement Control of Upper Extremity Prostheses,” 1995.

[18] A. Phinyomark, P. Phukpattaranont, and C. Limsakul, “Feature reduction and selection for EMG signal classification,” *Expert Systems with Applications*, vol. 39, no. 8, pp. 7420–7431, Jun. 2012, doi: 10.1016/j.eswa.2012.01.102.

[19] B. Karlık, “Machine Learning Algorithms for Characterization of EMG Signals,” *International Journal of Information and Electronics Engineering*, vol. 4, no. 3, 2014, doi: 10.7763/ijiee.2014.v4.433.

[20] S. El-Khoury *et al.*, *EMG-based learning approach for estimating wrist motion*. 2015. doi: 10.0/Linux-x86_64.

[21] H. B. Xie, Y. P. Zheng, J. Y. Guo, X. Chen, and J. Shi, “Estimation of wrist angle from sonomyography using support vector machine and artificial neural network models,” *Medical Engineering and Physics*, vol. 31, no. 3, pp. 384–391, Apr. 2009, doi: 10.1016/j.medengphy.2008.05.005.

[22] Jun Shi, “SVM for Estimation of Wrist Angle from Sonomyography And SEMG Signals”.

[23] D. Xiong, D. Zhang, X. Zhao, and Y. Zhao, “Deep Learning for EMG-based Human-Machine Interaction: A Review,” *IEEE/CAA Journal of Automatica Sinica*, vol. 8, no. 3, pp. 512–533, Mar. 2021, doi: 10.1109/JAS.2021.1003865.

[24] A. Ameri, M. A. Akhaee, E. Scheme, and K. Englehart, “Regression convolutional neural network for improved simultaneous EMG control,” *Journal of Neural Engineering*, vol. 16, no. 3, Apr. 2019, doi: 10.1088/1741-2552/ab0e2e.

[25] J. M. Hahne *et al.*, “Linear and nonlinear regression techniques for simultaneous and proportional myoelectric control,” *IEEE Transactions on Neural Systems and Rehabilitation Engineering*, vol. 22, no. 2, pp. 269–279, 2014, doi: 10.1109/TNSRE.2014.2305520.

[26] “Forearm muscles.” [Online]. Available: https://www.howtorelief.com/forearm-muscles-origin-insertion-nerve-supply-action/

[27] “Range of Joint Motion Evaluation Chart NAME OF PATIENT CLIENT IDENTIFICATION NUMBER.”

[28] “gForce EMG Armband User Guide,” 2015. [Online]. Available: www.oymotion.com

[29] “oymotion github”, Accessed: Feb. 11, 2022. [Online]. Available: https://oymotion.github.io/APPs/oym8CHWave/

[30] K. D. N. Oberländer, “Inverse Kinematics: Joint Considerations and the Maths for Deriving Anatomical Angles Inertial Measurement Unit (IMU) Technology IMU Tech,” 2015.

[31] “NGIMU User Manual,” 2016. [Online]. Available: www.x-io.co.uk

[32] Y.-B. Jia, “Quaternions and Rotations *,” 2013.

[33] N. Parajuli *et al.*, “Real-time EMG based pattern recognition control for hand prostheses: A review on existing methods, challenges and future implementation,” *Sensors (Switzerland)*, vol. 19, no. 20. MDPI AG, Oct. 02, 2019. doi: 10.3390/s19204596.

[34] A. Ullah, S. Ali, I. Khan, M. A. Khan, and S. Faizullah, “Effect of Analysis Window and Feature Selection on Classification of Hand Movements Using EMG Signal,” Feb. 2020, [Online]. Available: http://arxiv.org/abs/2002.00461

[35] O. W. Samuel *et al.*, “Intelligent EMG pattern recognition control method for upper-limb multifunctional prostheses: Advances, current challenges, and future prospects,” *IEEE Access*, vol. 7, pp. 10150–10165, 2019, doi: 10.1109/ACCESS.2019.2891350.

[36] L. H. Smith, L. J. Hargrove, B. A. Lock, and T. A. Kuiken, “Determining the optimal window length for pattern recognition-based myoelectric control: Balancing the competing effects of classification error and controller delay,” *IEEE Transactions on Neural Systems and Rehabilitation Engineering*, vol. 19, no. 2, pp. 186–192, Apr. 2011, doi: 10.1109/TNSRE.2010.2100828.

[37] T. R. Farrell and R. F. Weir, “The optimal controller delay for myoelectric prostheses,” *IEEE Transactions on Neural Systems and Rehabilitation Engineering*, vol. 15, no. 1, pp. 111–118, Mar. 2007, doi: 10.1109/TNSRE.2007.891391.

[38] M. Asghari Oskoei and H. Hu, “Myoelectric control systems-A survey,” *Biomedical Signal Processing and Control*, vol. 2, no. 4. Elsevier BV, pp. 275–294, 2007. doi: 10.1016/j.bspc.2007.07.009.

[39] B. Hudgins, P. Parker, and R. N. Scott, “A New Strategy for Multifunction Myoelectric Control,” *IEEE Transactions on Biomedical Engineering*, vol. 40, no. 1, pp. 82–94, 1993, doi: 10.1109/10.204774.

[40] S. Abbaspour, A. Naber, M. Ortiz-catalan, H. Gholamhosseini, and M. Lindén, “Real-time and offline evaluation of myoelectric pattern recognition for the decoding of hand movements,” *Sensors*, vol. 21, no. 16, Aug. 2021, doi: 10.3390/s21165677.

[41] M. Ortiz-Catalan, “Cardinality as a highly descriptive feature in myoelectric pattern recognition for decoding motor volition,” *Frontiers in Neuroscience*, vol. 9, no. OCT, 2015, doi: 10.3389/fnins.2015.00416.

[42] A. Phinyomark, C. Limsakul, and P. Phukpattaranont, “EMG FEATURE EXTRACTION FOR TOLERANCE OF 50 HZ INTERFERENCE,” 2009. [Online]. Available: http://icet2009.ftn.ns.ac.yu

[43] M. B. I. Reaz, M. S. Hussain, and F. Mohd-Yasin, “Techniques of EMG signal analysis: Detection, processing, classification and applications,” *Biological Procedures Online*, vol. 8, no. 1, pp. 11–35, Mar. 2006, doi: 10.1251/bpo115.

[44] S. Karlsson, J. Yu, and M. Akay, “Enhancement of spectral analysis of myoelectric signals during static contractions using wavelet methods,” *IEEE Transactions on Biomedical Engineering*, vol. 46, no. 6, pp. 670–684, 1999, doi: 10.1109/10.764944.

[45] A. L. Boulesteix, S. Janitza, J. Kruppa, and I. R. König, “Overview of random forest methodology and practical guidance with emphasis on computational biology and

bioinformatics," *Wiley Interdisciplinary Reviews: Data Mining and Knowledge Discovery*, vol. 2, no. 6, pp. 493–507, Nov. 2012, doi: 10.1002/widm.1072.

[46] "Random Forest scheme", Accessed: Feb. 11, 2022. [Online]. Available: https://medium.com/swlh/random-forest-and-its-implementation-71824ced454f

[47] F. S. Botros, A. Phinyomark, and E. J. Scheme, "Electromyography-Based Gesture Recognition: Is It Time to Change Focus from the Forearm to the Wrist?," *IEEE Transactions on Industrial Informatics*, vol. 18, no. 1, pp. 174–184, Jan. 2022, doi: 10.1109/TII.2020.3041618.